

High-harmonic generation in diatomic molecules: a quantum-orbit analysis of the interference patterns

C. Figueira de Morisson Faria

*Department of Physics and Astronomy, University College London,
Gower Street, London WC1E 6BT, United Kingdom*

(Dated: February 1, 2008)

We perform a detailed analysis of high-order harmonic generation in diatomic molecules within the strong-field approximation, with emphasis on quantum-interference effects. Specifically, we investigate how the different types of electron orbits, involving one or two centers, affect the interference patterns in the spectra. We also briefly address the influence of the choice of gauge, and of the initial and final electronic bound states on such patterns. For the length-gauge SFA and undressed bound states, there exist additional terms, which can be interpreted as potential energy shifts. If, on the one hand, such shifts alter the potential barriers through which the electron initially tunnels, and may lead to a questionable physical interpretation of the features encountered, on the other hand they seem to be necessary in order to reproduce the overall maxima and minima in the spectra. Indeed, for dressed electronic bound states in the length gauge, or undressed bound states in the velocity gauge, for which such shifts are absent, there is a breakdown of the interference patterns. In order to avoid such a problem, we provide an alternative pathway for the electron to reach the continuum, by means of an additional attosecond-pulse train. A comparison of the purely monochromatic case with the situation for which the attosecond pulses are present suggests that the patterns are due to the interference between the electron orbits which finish at different centers, regardless of whether one or two centers are involved.

I. INTRODUCTION

In the past few years, high-order harmonic generation (HHG) and above-threshold ionization (ATI) from aligned molecules in strong laser fields of femtosecond duration have proven to be a powerful tool for resolving, or even controlling, processes in the subfemtosecond and subangstrom scale. For instance, one may employ HHG and ATI in the tomographic reconstruction of molecular orbitals [1], and in the attosecond probing of dynamic changes in molecules [2].

This is possible due to the fact that the physical mechanisms governing both phenomena take place in a fraction of the laser period, i.e., within hundreds of attoseconds [3], and involve the recombination or the elastic scattering of an electron with its parent molecule [4]. Thereby, high-order harmonics or high-energy photoelectrons, respectively, are generated. Thus, the spectral features are highly dependent on the spatial configuration of the ions with which the electron rescatters or recombines, and yield patterns which are characteristic of the molecule. Furthermore, they also depend on the alignment angle of the molecule, with respect to the laser-field polarization.

Due to their simplicity, in particular diatomic molecules have been investigated, and minima and maxima have been encountered in their HHG and ATI spectra. Such patterns have been observed both theoretically [5, 6, 7, 8, 9, 10, 11, 12, 13, 14, 15, 16, 17, 18] and experimentally [19], and have been attributed to the interference between high-order harmonics or photoelectrons generated at different centers in the molecule. They are, in a sense, the microscopic counterpart of those obtained in a double-slit experiment. Furthermore, the energy positions of the maxima and min-

ima depend on the alignment angle and on the inter-nuclear distance and, additionally, reflect the bonding or antibonding nature of the highest occupied molecular orbitals in question [14, 15, 18]. Such features have been studied either numerically, by solving the time-dependent Schrödinger equation (TDSE) [14, 15, 18], or semi-analytically, by employing the strong-field approximation (SFA) [5, 6, 7, 8, 9, 10, 11, 12, 13, 16, 17]. In particular, in [15], the contributions to the yield from each molecular center have been singled out within a TDSE computation. Therein, it has been explicitly shown that the maxima and minima in the spectra are obtained due to the interference between contributions from different centers, in agreement with the double-slit model in [15, 18].

Specifically in the SFA framework, the transition amplitude can be written as a multiple integral, with a semiclassical action and slowly-varying prefactors. The structure of the molecule (and thus its double-slit character) can be either incorporated in the prefactors or in the action. The latter approach also takes into account processes in which an electron rescatters or recombines with a center in the molecule different from the site of its release [5, 9, 10, 11, 13].

An open question is, however, which types of electron orbits are responsible for specific interference features. For instance, are the dips and maxima originated by the interference between orbits in which the electron leaves and returns to the same center (regardless of which), or between those in which the electron leaves one atom and recombines with the other? On the other hand, it could also be that the interference patterns result from the combined effect of all such orbits, and one is not able to attribute them to specific sets.

Since the strong-field approximation is a semi-analytical method, and allows an immediate association with the classical orbits of an electron returning to its parent molecule, it appears to be an ideal tool for tackling this problem. This approximation, however, possesses several drawbacks. First, the SFA is gauge dependent, which leads to different pre-factors and action, depending on whether the velocity gauge or the length gauge is taken. Second, even for a specific gauge, the precise expressions for the pre-factors are not agreed upon, and some of them lead to interference patterns which are in disagreement with the experiments, and with results from other methods [15, 20].

The main objective of this work is to make a detailed assessment of the contributions and relevance of the different types of recombination scenarios to the above-mentioned interference patterns, within the Strong-Field Approximation, for a diatomic molecule. Throughout the paper, we approximate the strong, infra-red field by a linearly polarized monochromatic wave $\mathbf{E}(t) = E_0 \sin(\omega t) \mathbf{e}_x$, and consider a linear combination of atomic orbitals (LCAO approximation). In general, we consider that the electron reaches the continuum by tunneling ionization. As an exception, however, we also take an attosecond-pulse train superposed to the monochromatic wave [21, 22, 23, 24]. The attosecond-pulse train provides an additional pathway for the electron to reach the continuum, and, recently, has proven to be a powerful tool in order to control high-order harmonic generation [21, 23, 24] and above-threshold ionization [22, 23]. In the context of the present work, it is a convenient way to avoid problems related to spurious potential-energy shifts. These shifts are present in the length gauge and artificially modify the potential barrier through which the electron tunnels. Hence, they may lead to a questionable physical interpretation, what the relevance of the different sets of orbits to the patterns concerns.

This paper is organized as follows. In Sec. II, we discuss the strong-field approximation transition amplitude for high-order harmonic generation, starting from the general expressions (Sec. II A), and, subsequently, addressing the specific situation of a diatomic molecule in the LCAO approximation (Sec. II B). Thereby, we consider the situation for which the structure of the molecule is either incorporated in the pre-factor, or in the semiclassical action, in the presence and absence of the attosecond-pulse train. When discussing the former case, we emphasize the role of the overlap integrals, in which the dipole moment and the atomic wave functions are localized at different centers in the molecule. In the latter case, we follow the model in Ref. [11], for a purely monochromatic driving field, and our previous work [23] when the attosecond pulses are present, very closely. Subsequently (Sec. III), we investigate the interference patterns. Finally, in Sec. IV we summarize the paper and state our main conclusions.

II. TRANSITION AMPLITUDES

A. General expressions

In general, the strong-field approximation (SFA) consists in neglecting the influence of the laser field when the electron is bound, the atomic or molecular binding potential when the electron is in the continuum and the internal structure of the system in question, i.e., contributions from its excited bound states. The SFA transition amplitude for high-order harmonic generation reads, in the specific formulation of Ref. [26] and in atomic units,

$$b_\Omega = i \int_{-\infty}^{\infty} dt \int_{-\infty}^t dt' \int d^3 p d_{\text{rec}}^*(\tilde{\mathbf{p}}(t)) d_{\text{ion}}(\tilde{\mathbf{p}}(t')) \exp[iS(t, t', \Omega, \mathbf{k})] + c.c., \quad (1)$$

with the action

$$S(t, t', \Omega, \mathbf{p}) = -\frac{1}{2} \int_{t'}^t [\mathbf{p} + \mathbf{A}(\tau)]^2 d\tau - I_p(t - t') + \Omega t \quad (2)$$

and the prefactors $d_{\text{rec}}(\tilde{\mathbf{p}}(t)) = \langle \tilde{\mathbf{p}}(t) | \mathcal{O}_{\text{dip}} \cdot \mathbf{e}_x | \psi_0 \rangle$ and $d_{\text{ion}}(\tilde{\mathbf{p}}(t')) = \langle \tilde{\mathbf{p}}(t') | H_{\text{int}}(t') | \psi_0 \rangle$. In the above equations, \mathcal{O}_{dip} , \mathbf{e}_x , $H_{\text{int}}(t')$, I_p , and Ω denote the dipole operator, the laser-polarization vector, the interaction with the field, the ionization potential, and the harmonic frequency, respectively. The explicit expressions for $\tilde{\mathbf{p}}(t)$ are gauge dependent, and will be given below. The above-stated equation describes a physical process in which an electron, initially in a field-free bound-state $|\psi_0\rangle$, is coupled to a Volkov state $|\tilde{\mathbf{p}}(t')\rangle$ by the interaction $H_{\text{int}}(t')$ of the system with the field. Subsequently, it propagates in the continuum and is driven back towards its parent ion, with which it recombines at a time t , emitting high-harmonic radiation of frequency Ω . In Eq. (1), additionally to the above-mentioned assumptions, the further approximation of considering only transitions from a bound state to a Volkov state in the dipole moment has been made. In the single atom case, this has been justified by the fact that the remaining contributions, from the so-called “continuum-to-continuum” transitions, were very small. For a discussion of the various formulations of the SFA see, e.g., [25, 26, 27] and in particular [28].

Due to the fact that it can be carried out almost entirely analytically, the SFA is a very powerful approach. It possesses, however, the main drawback of being gauge-dependent (for general discussions see, e.g., Ref. [30], and for the specific case of molecules, Ref. [11]). Apart from the obvious fact that the interaction Hamiltonians $H_{\text{int}}(t')$, which are present in $d_{\text{ion}}(\tilde{\mathbf{p}}(t'))$, are different in the length and velocity gauges [31], in most computations where the SFA is employed, *field-free* bound states are taken, which are not gauge equivalent. Indeed, a field-free bound state $|\psi_0^{(L)}\rangle$ in the length gauge would be gauge equivalent to the field-dressed state $|\psi_0^{(V)}\rangle = \chi_{v \leftarrow l} |\psi_0^{(L)}\rangle$ in the velocity gauge, with $\chi_{v \leftarrow l} =$

$\exp[i\mathbf{A}(t) \cdot \mathbf{r}]$. Such a phase shift causes a translation $\mathbf{p} \rightarrow \mathbf{p} - \mathbf{A}(t)$ on a momentum eigenstate $|\mathbf{p}\rangle$. Hence, for field-free bound states in both gauges it leads to different dipole matrix elements $d_{\text{rec}}(\tilde{\mathbf{p}}(t))$ and $d_{\text{ion}}(\tilde{\mathbf{p}}(t))$. Explicitly, in the length gauge $\tilde{\mathbf{p}}(t) = \mathbf{p} + \mathbf{A}(t)$, while in the velocity gauge $\tilde{\mathbf{p}}(t) = \mathbf{p}$.

For computations involving a single atom, the latter artifact can be avoided by placing the system at the origin of the coordinate system. For systems composed of several centers, such as molecules, however, this ambiguity will always be present. Indeed, in the literature, different results have been reported for molecular SFA computations in the velocity and in the length gauge [7, 8, 11, 17]. In recent, modified versions of the length-gauge SFA, this problem has been eliminated for ATI by considering the initial bound state $|\tilde{\psi}_0^{(L)}\rangle = \exp[-i\mathbf{A}(t') \cdot \mathbf{r}] |\psi_0^{(L)}\rangle$. Such a state is gauge-equivalent to a field-free bound state in the velocity gauge, and, physically, may be interpreted as a field-dressed state, in which the laser-field polarization is included [17, 32]. For HHG, one may proceed in a similar way, with the main difference that the dressing should also be included in the final state, with which the electron recombines. In the dressed modified SFA, $\tilde{\mathbf{p}}(t) = \mathbf{p}$.

B. Diatomic molecules

We will now apply the SFA to a diatomic molecule. For this purpose, we will consider the simplest scenario, namely a one-electron system and frozen nuclei. Furthermore, we will assume that the molecular orbital from which the electron is released and with which it may recombine is a linear combination of atomic orbitals (LCAO approximation). Explicitly, the molecular bound-state wave function reads

$$\psi_0(r) = C_\psi(\psi_0^{(1)}(\mathbf{r}_1) + \epsilon\psi_0^{(2)}(\mathbf{r}_2)), \quad (3)$$

where $\epsilon = \pm 1$, $\mathbf{r}_1 = \mathbf{r} - \mathbf{R}/2$, and $\mathbf{r}_2 = \mathbf{r} + \mathbf{R}/2$ denote the positions of the centers C_1 and C_2 , respectively, and C_ψ is a normalization constant. For homonuclear molecules, which we will consider here, $\psi_0^{(1)} = \psi_0^{(2)} = \varphi_0$. The positive and negative signs for ϵ correspond to bonding and antibonding orbitals, respectively. Within this context, there exist two main approaches for computing high-order harmonic spectra, which will be discussed next.

1. Prefactors

The simplest and most widely used [6, 7, 8, 12, 15, 17, 20] approach is to incorporate the structure of the molecules in the prefactors $d_{\text{rec}}(\tilde{\mathbf{p}}(t))$ and $d_{\text{ion}}(\tilde{\mathbf{p}}(t))$, and to employ the same action $S(t, t', \Omega, \mathbf{p})$ as in the single-atom case. The multiple integral in the transition amplitude (1) can then either be solved numeri-

cally, or using saddle point methods [29]. The latter procedure can be applied for high enough intensities and low enough frequencies, and consists in approximating (1) by its asymptotic expansion around the coordinates $(t_s, t'_s, \mathbf{p}_s)$ for which $S(t, t', \Omega, \mathbf{p})$ is stationary. This implies that $\partial_t S(t, t', \Omega, \mathbf{p}) = \partial_{t'} S(t, t', \Omega, \mathbf{p}) = 0$ and $\partial_{\mathbf{p}} S(t, t', \Omega, \mathbf{p}) = \mathbf{0}$. In this paper, we employ the specific saddle-point approximations discussed in Ref. [33].

For a single atom placed at the origin of the coordinate system, this leads to the equations

$$[\mathbf{p} + \mathbf{A}(t')]^2 = -2I_p, \quad (4)$$

$$\int_{t'}^t d\tau [\mathbf{p} + \mathbf{A}(\tau)] = 0, \quad (5)$$

and

$$2(\Omega - I_p) = [\mathbf{p} + \mathbf{A}(t)]^2. \quad (6)$$

Eq. (4) expresses the conservation of energy at the time t' at which the electron reaches the continuum by tunneling ionization. This equation possesses no real solution, which reflects the fact that tunneling has no classical counterpart. In the limit $I_p \rightarrow 0$, one obtains such a condition for a classical particle reaching the continuum with vanishing drift velocity. Eq. (5) constrains the intermediate momentum of the electron, so that it returns to its parent ion, and, finally, Eq. (6) describes the conservation of energy at a later time t , when the electron recombines with its parent ion and a high-frequency photon of frequency Ω is generated.

The matrix element $d_{\text{rec}}(\tilde{\mathbf{p}}) = \langle \tilde{\mathbf{p}} | \mathcal{O}_{\text{dip}} \cdot \mathbf{e}_x | \psi_0 \rangle$ then reads

$$d_{\text{rec}}(\tilde{\mathbf{p}}) = \frac{C_\psi}{(2\pi)^{3/2}} \left[e^{i\tilde{\mathbf{p}} \cdot \mathbf{R}/2} \mathcal{I}(\mathbf{r}_1) + \epsilon e^{-i\tilde{\mathbf{p}} \cdot \mathbf{R}/2} \mathcal{I}(\mathbf{r}_2) \right], \quad (7)$$

where

$$\mathcal{I}(\mathbf{r}_j) = \int \mathcal{O}_{\text{dip}}\left(\frac{\mathbf{r}_1 + \mathbf{r}_2}{2}\right) \cdot \mathbf{e}_x \exp[i\tilde{\mathbf{p}} \cdot \mathbf{r}_j] \varphi_0(\mathbf{r}_j) d^3r_j, \quad (8)$$

and $\mathcal{O}_{\text{dip}}(\frac{\mathbf{r}_1 + \mathbf{r}_2}{2})$ is the dipole moment. In the length gauge, which we are mostly adopting in this paper, $\tilde{\mathbf{p}}(t) = \mathbf{p} + \mathbf{A}(t)$. Unless strictly necessary, in order to simplify the notation, we do not include the time dependence in $\tilde{\mathbf{p}}$. The dipole moment can be written in several forms. If one considers the length form a natural choice is $\mathcal{O}_{\text{dip}}^{(l)}(\mathbf{r}) = -e\mathbf{r} + e\mathbf{r}_1 + e\mathbf{r}_2 = e\mathbf{r}$. Other possibilities are to consider the operator \mathcal{O}_{dip} in its velocity and acceleration forms [20, 34].

Inserting $\mathcal{O}_{\text{dip}}(\mathbf{r})$ in Eq. (8) yields

$$\mathcal{I}(\mathbf{r}_j) \propto \mathcal{I}_j(\mathbf{r}_j) + \mathcal{I}_{j\nu}(\mathbf{r}_j), \quad \text{with } j = 1, 2 \text{ and } \nu \neq j, \quad (9)$$

where

$$\mathcal{I}_j(\mathbf{r}_j) = \int \mathcal{O}_{\text{dip}}(r_j) \cdot \mathbf{e}_x \exp[i\tilde{\mathbf{p}} \cdot \mathbf{r}_j] \varphi_0(\mathbf{r}_j) d^3r_j \quad (10)$$

and

$$\mathcal{I}_{j\nu}(\mathbf{r}_j) = \int \mathcal{O}_{\text{dip}}(r_\nu) \cdot \mathbf{e}_x \exp[i\tilde{\mathbf{p}} \cdot \mathbf{r}_j] \varphi_0(\mathbf{r}_j) d^3 r_j, \nu \neq j. \quad (11)$$

Specifically, if the dipole is in the length form, the above-stated integrals read

$$\mathcal{I}_j(\mathbf{r}_j) = -\frac{i}{2} \partial_{\tilde{p}_x} \phi(\tilde{\mathbf{p}}) \quad (12)$$

and

$$\mathcal{I}_{j\nu}(\mathbf{r}_j) = \frac{1}{2} (-i \partial_{p_x} \phi(\tilde{\mathbf{p}}) + \epsilon_j R_x \phi(\tilde{\mathbf{p}})), \quad (13)$$

where

$$\phi(\tilde{\mathbf{p}}) = \int \exp[i\tilde{\mathbf{p}} \cdot \mathbf{r}_j] \varphi_0(\mathbf{r}_j) d^3 r_j. \quad (14)$$

In $\mathcal{I}_{j\nu}$, $\epsilon_j = +1$ for $j = 1$ and $\epsilon_j = -1$ for $j = 2$. Eq. (7) is then explicitly written as

$$d_{\text{rec}}^{(b)}(\tilde{\mathbf{p}}) = \frac{2iC_\psi}{(2\pi)^{3/2}} \left[-\cos(\vartheta) \partial_{p_x} \phi(\tilde{\mathbf{p}}) + \frac{R_x}{2} \sin(\vartheta) \phi(\tilde{\mathbf{p}}) \right], \quad (15)$$

for bonding molecular orbitals (i.e., $\epsilon > 0$), or

$$d_{\text{rec}}^{(a)}(\tilde{\mathbf{p}}) = \frac{2C_\psi}{(2\pi)^{3/2}} \left[\sin(\vartheta) \partial_{p_x} \phi(\tilde{\mathbf{p}}) - \frac{R_x}{2} \cos(\vartheta) \phi(\tilde{\mathbf{p}}) \right], \quad (16)$$

in the antibonding case (i.e., $\epsilon < 0$), with $\vartheta = \tilde{\mathbf{p}} \cdot \mathbf{R}/2$.

In Eqs. (15) and (16), the terms with a purely trigonometric dependence on the internuclear distance yield the double-slit condition in [18]. The maxima and minima in the spectra which are caused by this condition are expected to occur for

$$\tilde{\mathbf{p}} \cdot \mathbf{R} = 2n\pi \text{ and } \tilde{\mathbf{p}} \cdot \mathbf{R} = (2n+1)\pi, \quad (17)$$

respectively, for bonding molecular orbitals (i.e., $\epsilon > 0$). For antibonding orbitals, the conditions are reversed, i.e., the maxima occur for the odd multiples of π and the minima for the even multiples. If the velocity gauge is taken, the above stated conditions hold for $\tilde{\mathbf{p}}(t) = \mathbf{p}$, instead of $\tilde{\mathbf{p}}(t) = \mathbf{p} + \mathbf{A}(t)$. This is due to the fact that the initial and final free-field states are not gauge equivalent, as discussed in Sec. IIA.

The remaining terms grow linearly with the projection R_x of the internuclear distance along the direction of the laser-field polarization, and may lead to unphysical results [11, 20]. For this reason, they are sometimes neglected in the integrals $\mathcal{I}_{j\nu}(\mathbf{r}_j)$ [16]. There exists, however, no rigorous justification for such a procedure. Indeed, only recently, it has been shown that such terms can be eliminated by considering an additional interaction which depends on the nuclear coordinate. This interaction is present in a modified molecular SFA, in its dressed and undressed versions [17], and leads to contributions which cancel out the linear term in R_x .

In the length gauge, if the length form of \mathcal{O}_{dip} is taken, $d_{\text{rec}}(\tilde{\mathbf{p}}(t)) = d_{\text{ion}}(\tilde{\mathbf{p}}(t'))$, with $\tilde{\mathbf{p}}(t) = \mathbf{p} + \mathbf{A}(t)$, while in the velocity gauge,

$$d_{\text{ion}}^{(b)}(\tilde{\mathbf{p}}) = \frac{C_\psi [\mathbf{p} + \mathbf{A}(t')]^2}{(2\pi)^{3/2}} \cos(\vartheta) \phi(\tilde{\mathbf{p}}), \quad (18)$$

or

$$d_{\text{ion}}^{(a)}(\tilde{\mathbf{p}}) = -i \frac{C_\psi [\mathbf{p} + \mathbf{A}(t')]^2}{(2\pi)^{3/2}} \sin(\vartheta) \phi(\tilde{\mathbf{p}}), \quad (19)$$

with $\tilde{\mathbf{p}}(t) = \mathbf{p}$, for bonding and antibonding molecular orbitals, respectively.

2. Modified saddle-point equations

Physically, if one employs the pre-factors (15) and (16), this means that one is not modifying the saddle-point equations (4)-(6). Therefore, the orbits along which the electron is moving in the continuum remain the same as in the single-center case. This approach is questionable in several ways. From the technical viewpoint, there is no guarantee that such pre-factors are slowly varying, as compared to the semiclassical action, especially for large internuclear distances [9, 11]. Furthermore, in general, they do not incorporate processes in which the electron leaves one center of the molecule and recombines with the other, which, physically, are expected to be present in molecular HHG [11].

A slightly more sophisticated approach is to exponentiate the pre-factors obtained in the two-center case and incorporate the terms in $\tilde{\mathbf{p}} \cdot \mathbf{R}/2$ in the action. This procedure has been adopted in [11] and will be closely followed in this work. For the sake of simplicity, we will consider the modified prefactor

$$\tilde{d}_{\text{rec}}^{(b)}(\tilde{\mathbf{p}}) = -\frac{2iC_\psi}{(2\pi)^{3/2}} \left[\cos\left(\tilde{\mathbf{p}} \cdot \frac{\mathbf{R}}{2}\right) \partial_{\tilde{p}_x} \phi(\tilde{\mathbf{p}}) \right], \quad (20)$$

for which the second term in Eq. (13) is absent. Eq. (20) is also very similar to the dipole matrix element in the velocity form, apart from the fact that, in the latter case, $\partial_{\tilde{p}_x} \phi(\tilde{\mathbf{p}})$ is replaced by $\tilde{\mathbf{p}} \phi(\tilde{\mathbf{p}})$ [20]. In the expression for the antibonding case, the cosine term in (20) should be replaced by $\sin(\tilde{\mathbf{p}} \cdot \mathbf{R}/2)$.

This leads to the sum

$$M = \sum_{j=1}^2 \sum_{\nu=1}^2 M_{j\nu} \quad (21)$$

of the transition amplitudes

$$M_{j\nu} = \frac{C_\psi}{(2\pi)^{3/2}} \int_0^t dt' \int dt \int d^3 p \eta(\mathbf{p}, t, t') \times \exp[iS_{j\nu}(\mathbf{p}, \Omega, t, t')], \quad (22)$$

with $\eta(\mathbf{p}, t, t') = [\partial_{\tilde{p}_x} \phi(\tilde{\mathbf{p}}(t))]^* \partial_{\tilde{p}_x} \phi(\tilde{\mathbf{p}}(t'))$. The terms $S_{j\nu}$ correspond to a modified action, which incorporates the structure of the molecule.

Explicitly, for the undressed length-gauge SFA,

$$S_{jj} = S(\mathbf{p}, \Omega, t, t') + (-1)^{j+1} \xi_1(R, t, t') \quad (23)$$

and

$$S_{j\nu} = S(\mathbf{p}, \Omega, t, t') + (-1)^{\nu+1} \xi_2(R, t, t'), \quad \nu \neq j, \quad (24)$$

where $\xi_1(R, t, t') = [\mathbf{A}(t) - \mathbf{A}(t')] \cdot \mathbf{R}/2$ and $\xi_2(R, t, t') = \mathbf{p} \cdot \mathbf{R} + [\mathbf{A}(t) + \mathbf{A}(t')] \cdot \mathbf{R}/2$. Eq. (23) and (24) may be directly related to physical processes involving one or two centers in the molecule, respectively, as it will be discussed next.

For this purpose, we will solve the multiple integrals in (22) employing saddle-point methods. The conditions $\partial_{\mathbf{p}} S_{j\nu}(\mathbf{p}, \Omega, t, t') = \mathbf{0}$, $\partial_t S_{j\nu}(\mathbf{p}, \Omega, t, t') = 0$ and $\partial_{t'} S_{j\nu}(\mathbf{p}, \Omega, t, t') = 0$ upon the derivative of the action yield saddle-point equations, which, as in the previous section, can be related to the orbits of an electron recombining with the molecule. Explicitly, for the modified action S_{jj} , [Eq. (23)], the saddle-point equations read

$$\frac{[\mathbf{p} + \mathbf{A}(t')]^2}{2} = -I_p - \mathbf{E}(t') \cdot \mathbf{R}/2, \quad (25)$$

$$\frac{[\mathbf{p} + \mathbf{A}(t)]^2}{2} = \Omega - I_p + \mathbf{E}(t) \cdot \mathbf{R}/2, \quad (26)$$

for $j = 1$, or

$$\frac{[\mathbf{p} + \mathbf{A}(t')]^2}{2} = -I_p + \mathbf{E}(t') \cdot \mathbf{R}/2, \quad (27)$$

$$\frac{[\mathbf{p} + \mathbf{A}(t)]^2}{2} = \Omega - I_p - \mathbf{E}(t) \cdot \mathbf{R}/2, \quad (28)$$

for $j = 2$. The saddle point equations (25) and (27) correspond to the tunnel ionization process from center C_1 and C_2 , respectively. Curiously, both equations contain extra terms, if compared to equation (4) for the single-atom case. Such terms are dependent on the internuclear distance \mathbf{R} and the external laser field $\mathbf{E}(t')$ at the time the electron is freed, and may be interpreted as potential-energy shifts in the barrier through which the electron tunnels out. Similar terms are also observed in Eqs. (26) and (28) for the energy conservation at the time the electron recombines, as compared to the single-atom expression (6).

The remaining saddle point equation is given by the same expression as in the single-atom case, i.e., Eq. (5), and means that, for M_{11} and M_{22} , the electron is ejected and returns to the same center. If on the other hand, we consider the modified action (24), this yields

$$\int_{t'}^t [\mathbf{p} + \mathbf{A}(s)] ds \pm \mathbf{R} = 0, \quad (29)$$

which, physically, mean that the electron is leaving from one center and recombining with the other. The negative

and positive signs refer to the transition amplitudes M_{12} (center C_1 to center C_2) and M_{21} (center C_2 to center C_1), respectively. In the former case, the remaining saddle points are given by (25) and (28), i.e., the electron tunnels from C_1 and recombines with C_2 , whereas in the latter case they are given by (27) and (26), which physically, expresses the fact that the electron is ejected at C_2 and recombines with C_1 .

The energy shifts $\pm \mathbf{E}(\tau) \cdot \mathbf{R}/2$, $\tau = t, t'$ in (25)-(28) are absent in the velocity gauge SFA [11], and in a modified length-gauge SFA, in which the electric field polarization is incorporated in the initial and final electronic bound states. In both cases, the action S_{jj} , associated to orbits involving only one center, is given by the single-atom expression (2), which leads to the saddle-point equations (4)-(6). The action $S_{j\nu}$ related to two-center orbits reads

$$\tilde{S}_{j\nu} = S(\mathbf{p}, \Omega, t, t') + (-1)^{\nu+1} \mathbf{p} \cdot \mathbf{R}, \quad \nu \neq j. \quad (30)$$

The above-stated expression leads to the single-atom equations (4), (6) for tunneling and rescattering, together with the two-center return condition (29). The prefactors, however, are different in both cases. In the dressed modified length-gauge SFA, $\eta^D(\mathbf{p}, t, t') = [\partial_{p_x} \phi(\mathbf{p})]^* \partial_{p_x} \phi(\mathbf{p})$, while in the velocity gauge $\eta^V(\mathbf{p}, t, t') = [\partial_{p_x} \phi(\mathbf{p})]^* \phi(\mathbf{p}) [\mathbf{p} + \mathbf{A}(t')]^2/2$.

One should note that, within the specific model employed here, the physical process in which the electron moves directly from one center to the other, without reaching the continuum, is not being considered. Such a process leads to a strong set of harmonics in the low-energy range of the spectra. Since, however, we are focusing on the plateau harmonics, the contributions from this extremely short set of orbits are not of interest to the present discussion. For a detailed study of this case, see, e.g., [5, 10].

3. Additional attosecond pulses

The role of the energy shifts observed in (25)-(28) is not well understood. A way of eliminating such terms is to modify the length-gauge SFA and include the influence of the laser field in the initial and final states. However, even without such modifications, it is possible to provide an additional pathway for the electron to reach the continuum, so that, at least in the context of tunneling ionization, these shifts can be avoided. For instance, if the electron is ejected by a high-frequency photon, it does not have to tunnel through potential barriers with energy shifts whose physical meaning is not clear. Such a pathway can be provided by a time-delayed attosecond-pulse train $\mathbf{E}_h(t)$ superposed to a strong, near infra-red field $\mathbf{E}_l(t) = E_0 \sin \omega t \mathbf{e}_x$. Indeed, it has been recently shown that such pulses can be used to control the electron ejection in the continuum, and thus high-harmonic generation and above-threshold ionization [21, 22, 23].

In [23, 24], we employed such a scheme to control quantum-interference effects for high-harmonic genera-

tion and above-threshold ionization for the single-atom case, within the SFA framework. Our previous findings suggest that the probability of the electron reaching the continuum, in case it is ejected by the attosecond pulses, is roughly the same for all sets of orbits. Indeed, it appears that the sole, or at least main factor determining the intensities in the spectra is the excursion time of the electron in the continuum. In the specific case studied in [23], there was a set of very short orbits, which led to particularly strong harmonics. Therefore, an attosecond pulse train superposed to a strong laser field is an ideal setup to avoid any artifacts due to modified tunneling conditions.

In [23], we have approximated the attosecond pulse train by a sum of Dirac-Delta functions in the time domain. This yields

$$\mathbf{E}_h(t) = E_h \pi \sum_{n=0}^{\infty} \frac{(-1)^n}{\sigma(t)} \delta(t - \frac{n\pi}{\omega} - t_d) \epsilon_x, \quad (31)$$

where ω , E_h , and $\sigma(t)$ denote the laser field frequency, the attosecond-pulse strength and the train temporal envelope, respectively. This approximation is the limiting case for a train composed of an infinite set of harmonics, and has the main advantage of allowing an analytic treatment of the transition amplitudes involved up to at most one numerical integration. Furthermore, it is a reasonable asymptotic limit for pulses composed by a large high-harmonic set. We consider here $\sigma = \text{const}$, which, physically, corresponds to an infinitely long attosecond-pulse train. Clearly, the total field is given by $\mathbf{E}(t) = \mathbf{E}_l(t) + \mathbf{E}_h(t)$.

We will now assume that the attosecond pulses are the only cause of ionization and that the subsequent propagation of the electron in the continuum is determined only by the monochromatic field. Hence, $\mathbf{E}(t') \simeq \mathbf{E}_h(t')$ and $\mathbf{A}(t) \simeq \mathbf{A}_l(t)$ in Eqs. (1) and (22). This eliminates the integral over the ionization time in the transition amplitudes. Hence, the values for which the single atom-action $S(t, t', \Omega, \mathbf{k})$, or the modified action $S_{j\nu}$ is stationary must be determined only with respect to the variables t and \mathbf{p} . Physically this means that the recombination and return conditions remain the same, with regard to the purely monochromatic case, but that there is no longer a saddle-point equation constraining the initial electron momentum. In fact, the electron is being ejected in the continuum with any of the energies $N\omega - I_p$, since all harmonics composing the train are equivalent. For the other extreme limit, namely a high-frequency monochromatic wave, we refer to [24], where we provide a detailed discussion within the SFA.

Explicitly, if the action is not modified, these assumptions lead to the transition amplitude

$$M_h^{(D)} = \frac{i\pi C_\psi E_h}{\sigma(2\pi)^{3/2}} \sum_{n=0}^{\infty} (-1)^n \int_{-\infty}^{+\infty} dt \int d^3p \exp[iS(\mathbf{p}, \Omega, t, t')] \times d_{\text{rec}}^*(\tilde{\mathbf{p}}(t)) d_{\text{ion}}(\tilde{\mathbf{p}}(t')).$$

In case one considers the transition amplitudes (22), this yields

$$M_{j\nu} = \frac{i\pi C_\psi E_h}{\sigma(2\pi)^{3/2}} \sum_{n=0}^{\infty} (-1)^n \int_{-\infty}^{+\infty} dt \int d^3p \eta(\tilde{\mathbf{p}}, t, t') \times \exp[iS_{j\nu}(\mathbf{p}, \Omega, t, t')]. \quad (33)$$

In both equations, $t' = t_d + n\pi/\omega$. The saddle-point equations (5) and (6) for the single atom case can then be combined as

$$\sin \omega t - (-1)^n \sin \omega t_d = [\omega(t - t_d) - n\pi] \left(\cos \omega t \mp \sqrt{\frac{\Omega - I_p}{2U_p}} \right), \quad (35)$$

which will give the return times t . If, on the other hand, these equations are modified, it is possible to distinguish four main scenarios. Specifically, for the processes in which the electron leaves and returns to the same center, the saddle-point equations differ from (35) only in a shift $I_p \rightarrow I_p \pm \mathbf{E}_l(t) \cdot \mathbf{R}/2$. The negative and positive signs correspond to M_{11} and M_{22} , respectively. For the scenarios involving two centers, the saddle-point equations read

$$\sin \omega t - (-1)^n \sin \omega t_d + \epsilon \frac{R_x \omega}{2U_p} = [\omega(t - t_d) - n\pi] \left(\cos \omega t \mp \sqrt{\frac{\Omega - \tilde{I}_p}{2U_p}} \right), \quad (36)$$

with $\tilde{I}_p = I_p + \epsilon \mathbf{E}_l(t) \cdot \mathbf{R}/2$. The case $\epsilon = -1$ and $\epsilon = +1$ corresponds to M_{12} and M_{21} , respectively.

III. HARMONIC SPECTRA

We will now present high-harmonic spectra, in the presence and absence of the attosecond pulses. We restrict the electron ionization times to the first half cycle of the driving field. We also consider the six shortest pairs of orbits for the returning electron. Due to wave-packet spreading, the contributions from the remaining pairs are negligible [35]. For simplicity, we employ a bonding combination of 1s states, for which

$$\phi(\tilde{\mathbf{p}}) \sim \frac{1}{[\tilde{\mathbf{p}}^2 + 2I_p]^2}, \quad (37)$$

and assume that the molecule is aligned parallel to the laser-field polarization, so that $R_x = R$.

A. Prefactors

We will commence by considering the single-center action (2) and the prefactors discussed in the previous sec-

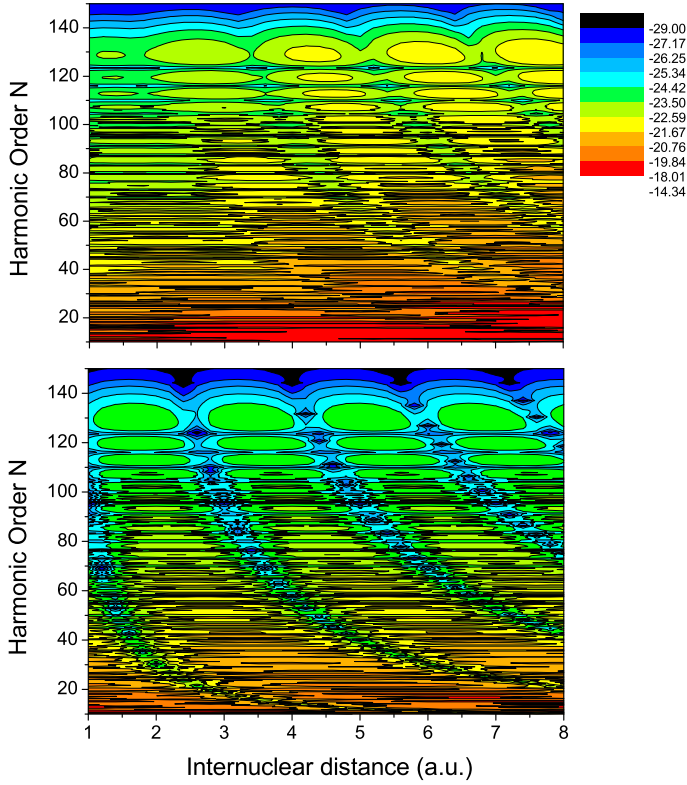


FIG. 1: (Color Online) High-harmonic spectra computed employing the single-atom orbits and two center prefactors, using a bonding ($\epsilon = +1$), linear combination of atomic orbitals, for internuclear distances $1 \text{ a.u.} \leq R \leq 8 \text{ a.u.}$. The upper and lower panels correspond to the dipole prefactors (15) and (20), respectively. The atomic system was chosen as H_2^+ , which was approximated by the linear combination of $1s$ atomic orbitals with $I_p = 0.5 \text{ a.u.}$. We took the driving field intensity and frequency to be $I = 1 \times 10^{15} \text{ W/cm}^2$, and $\omega = 0.057 \text{ a.u.}$, respectively.

tion. In Fig. 1, we depict high-harmonic spectra computed for a wide range of internuclear distances, employing the prefactor (15) or the modified expression (20), for which the linear term in R_x is absent [upper and lower panel, respectively]. The figure illustrates how the linear term masks the interference patterns. In fact, for $1 \leq R \leq 3 \text{ a.u.}$, it counterbalances the influence of the purely trigonometric term, and no clear minima and maxima are observed. As the internuclear distance increases, this term starts to play a dominant role, displacing the maxima and minima away from the double-slit condition (17). Furthermore, it seems that the patterns become more distinct with increasing harmonic order.

A rough estimate of the influence of each term in (15) on the spectra agrees with Fig. 1. Since the trigonometric functions in (15) are bounded, the ratio between the maxima caused by each term will be $\zeta = R |\cos \theta \phi(\tilde{\mathbf{p}}) / (2 \partial_{p_x} \phi(\tilde{\mathbf{p}}))|$, where θ is the alignment angle and $\phi(\tilde{\mathbf{p}})$ is given by Eq. (14). If $\zeta \simeq 1$, the maxima will possess the same order of magnitude and there will be

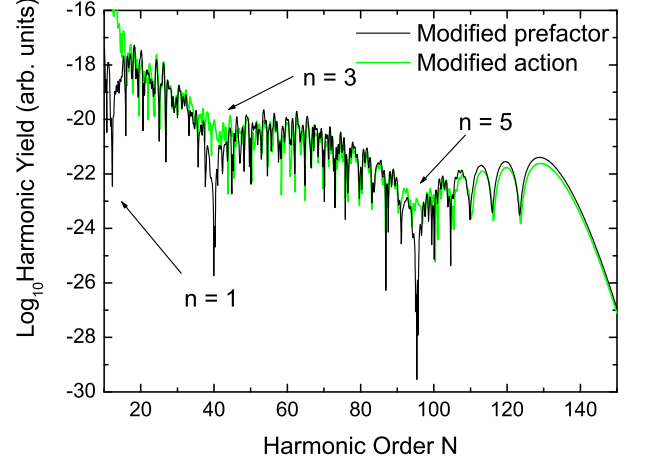


FIG. 2: (Color online) Spectra computed employing the single-atom orbits and two center prefactors (black thin lines), as compared to those obtained employing modified saddle-point equations (green thick lines). We consider here the modified length form (20) of the dipole operator, which excludes the term with a linear dependence on R_x . The atomic system was chosen as H_2^+ , which was approximated by the linear combination of $1s$ atomic orbitals with $I_p = 0.5 \text{ a.u.}$. The internuclear distance and the alignment angle are $R = 5 \text{ a.u.}$, and $\theta = 0$, respectively. The driving field intensity and frequency are given by $I = 1 \times 10^{15} \text{ W/cm}^2$, and $\omega = 0.057 \text{ a.u.}$, respectively. The interference minima are indicated by the arrows in the figure.

no noticeable modulation, while if $\zeta < 1$ the double-slit physical picture may still be reproduced. For $\zeta > 1$, however, one expects that the linear term in R will prevail. Hence, the critical value for the internuclear distance is $R_c = 2 |\sec \theta \partial_{p_x} \phi(\tilde{\mathbf{p}}) / \phi(\tilde{\mathbf{p}})|$. This expression depends on the bound states with which the electron recombines, and also on the harmonic energy. For instance, specifically for $1s$ states, $R_c \sim 4 \tilde{p}_x \sec \theta / (\tilde{\mathbf{p}}^2 + 2I_p)$. Above the ionization threshold, according to Eq. (6), $R_c \sim 2 \tilde{p}_x \sec \theta / \Omega$. Hence, one expects the linear term to be more prominent as the harmonic energy increases, leading to clearer, though incorrect, patterns. In order to avoid such problems, we will employ the prefactor (20) throughout.

In Fig. 2, we compare spectra computed using either the pre-factor (20) or modified saddle-point equations. Both spectra are very similar, with maxima and minima at harmonic frequencies $\Omega = I_p + n^2 \pi^2 / (2R_x^2)$, as expected from the double-slit condition. This similarity holds not only for the gross features, but, additionally, for the substructure caused by other types of quantum interference. Close to the minima, however, the yield from the latter case is larger. Nevertheless, the very good overall agreement shows that, in fact, the patterns obtained can also be interpreted as the result of the quantum interference between different types of electron orbits.

B. Interference effects

In order, however, to identify which sets of orbits cause the dips and the maxima, we will analyze the interference between their individual contributions. Such results are shown in Fig. 3. In the upper panels, we present the spectra computed from topologically similar sets of orbits, i.e., from processes involving only one, or two centers [panel 3.(a)]. In this case, the main interference patterns are absent. This strongly suggests that they are due to the quantum interference of topologically different sets of orbits: the orbits along which an electron leaves and returns to the same center, and those along which it reaches the continuum at one center and recombines with the other. Physically, this could be attributed to the fact that, in this case, there would be an appreciable phase difference between the two sets of orbits, since the latter are much longer than the former. This phase difference would cause the overall modulation.

Hence, there are two remaining possibilities. Concretely, the modulation can be due to the quantum interference either between processes in which the electron leaves from different centers and recombines with the same center (i.e., between the orbits which start at C_j and end at C_ν , with $\nu \neq j$, and those starting and ending at C_ν , and $j = 1, 2$), or between those in which an electron starts at the same center and recombines with different centers (i.e., the electron is ejected at C_j and recombines at C_ν , $\nu \neq j$, or it is freed and recombines at C_j , with $j = 1, 2$). In panel 3.(b), we consider the former processes, whereas in panel 3.(c) we depict the latter. Interestingly, only in case the electron leaves from the same center, the interference patterns are present. Furthermore, there is a difference in roughly four orders of magnitude between the two types of contributions. Such a difference is absent in the other cases. Additionally, the full contributions to the yield are practically indistinguishable from the transition probability $|M_{21} + M_{22}|^2$, from the orbits starting at C_2 .

In order to understand this better, one must have a closer look at the individual contributions from different sets of orbits, and, in particular their orders of magnitude. Such contributions, depicted in Panels (a) and (b) of Fig. 4, show that the transition probabilities $|M_{22}|^2$ and $|M_{21}|^2$, which correspond to the orbits starting from the center C_2 , are roughly four orders of magnitude larger than $|M_{12}|^2$ and $|M_{11}|^2$, i.e., than those from the orbits starting at C_1 . Therefore, it is not surprising that the yield is dominated by $|M_{21} + M_{22}|^2$ in the previous figure. Furthermore, these results exhibit no maxima and minima. Hence, they support the assumption that such features are due to the interference of different types of orbits. Finally, the contributions from orbits starting at the same center possess the same order of magnitude. This suggests that tunneling ionization is the main mechanism determining the relevance of a particular type of orbits to the spectra, and that are local differences in the barrier through which the electron must tunnel, depend-

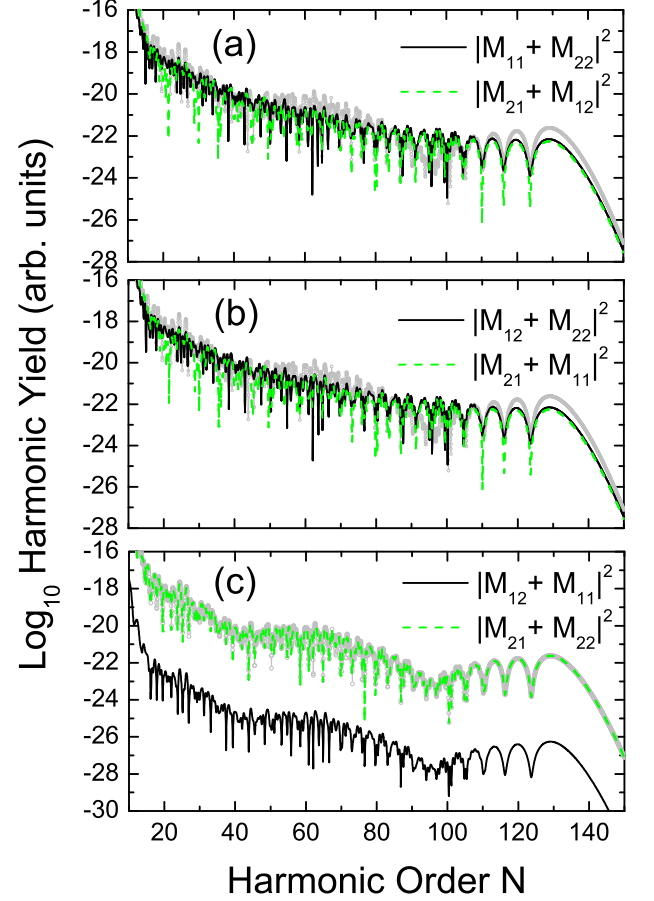


FIG. 3: (Color Online) Contributions to the high-harmonic yield from the quantum interference between different types of orbits, for internuclear distance $R = 5$ a.u. The remaining parameters are the same as in Fig. 3. Panel (a): Orbits involving similar scattering scenarios, i. e., $|M_{11} + M_{22}|^2$, and $|M_{12} + M_{21}|^2$. Panel (b): Orbits *ending* at the same center, i.e., $|M_{11} + M_{21}|^2$ and $|M_{12} + M_{22}|^2$. Panel (c): Orbits *starting* at the same center, i.e., $|M_{11} + M_{12}|^2$ and $|M_{21} + M_{22}|^2$. For comparison, the full contributions $|M_{21} + M_{22} + M_{11} + M_{12}|^2$ are displayed as the light gray circles in the picture.

ing on the center it starts from.

An inspection of the imaginary parts $\text{Im}[t']$ of the start times provides additional insight into this problem. Due to the fact that tunneling ionization is a process which has no classical counterpart, this quantity is always non-vanishing, even if the energy range in question is lower than the maximal harmonic energy. The larger $\text{Im}[t']$ is, the less probable it will be that tunneling ionization takes place. Such an interpretation has been successfully employed in [36] in order to determine the dominant pairs of orbits, in the context of nonsequential double ionization with few-cycle laser pulses, and will be also considered in this work. For that purpose, we will take the shortest

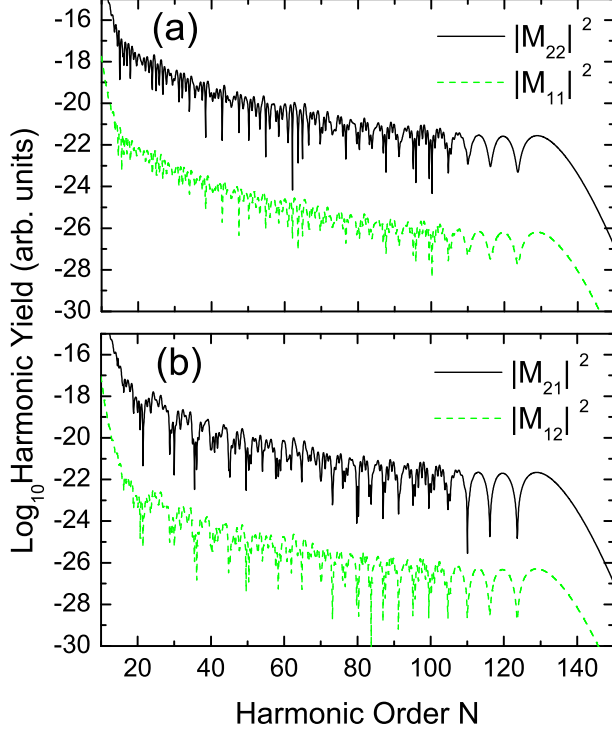


FIG. 4: (Color online) Contributions to the high-harmonic yield from specific types of orbits, for internuclear distance $R = 5$ a.u. The remaining parameters are the same as in Fig. 3. Panel (a): Yield from the orbits starting and ending at the same center, i. e., transition probabilities $|M_{11}|^2$ and $|M_{22}|^2$. Panel (b): Yield from the orbits starting and ending at different centers, i.e., transition probabilities $|M_{12}|^2$ and $|M_{21}|^2$.

pairs of orbits utilized in the computation of the transition probabilities in Fig. 4 and, for each case, display $\text{Im}[t']$. These are the dominant pairs of orbits. The longer pairs have a less significant influence on the spectra, due to the spreading of the electronic wave packet [35].

Such results are depicted in Fig. 5. Clearly, $\text{Im}[t']$ is around four times larger for the orbits starting from the center C_1 , as compared to those starting from C_2 . This means that, in order to reach the continuum, the electron must overcome a larger barrier if it comes from C_1 . Since, roughly speaking, the ionization probability per unit time decreases exponentially with $\text{Im}[t']$, one expects the contributions from the orbits starting from C_1 to be around four orders of magnitude smaller than those from the orbits starting at C_2 . An inspection of Fig. 4 shows that this is indeed the case.

The above-stated effect could, however, be an artifact of the strong-field approximation in the length gauge. Indeed, the terms $\pm \mathbf{E}(t') \cdot \mathbf{R}$ in the saddle-point equations (25) and (27) can be interpreted as potential en-

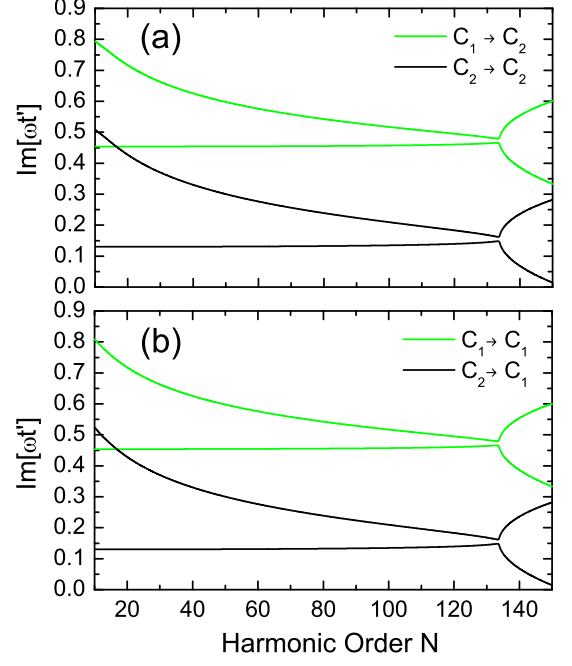


FIG. 5: (Color online) Imaginary parts of the start times t' of the shortest pairs of orbits, which contribute to the matrix elements M_{22} , and M_{12} , [panel (a)], and to M_{21} , and M_{11} [panel (b)], for the same field and atomic parameters as in the previous figure.

ergy shifts, due to the fact that the electron is displaced from the origin [11, 17]. Such terms increase or sink the potential barrier for C_1 or C_2 , respectively, and, consequently, change the orders of magnitude in the contributions starting from different centers. Even though, as a whole, the results match those obtained by other means, their physical interpretation is controversial.

One may, however, avoid this problem by providing an additional pathway for the electron to reach the continuum. For that purpose, we shall superpose a time-delayed attosecond pulse train to the strong laser field, employing the model discussed in Sec. II B 3 and in our previous work [23, 24]. The maximal harmonic energies for this specific model are strongly dependent on the time delay t_d between the attosecond-pulse train the infra-red field, extending from the ionization potential, for $\phi = 0.75\pi$ to $I_p + 1.8U_p$, for $\phi = n\pi$. Furthermore, there exist many intermediate delays, for which a double plateau is present. This substructure may be detrimental to the identification and physical interpretation of the interference patterns. In order to avoid such problems, we will consider here vanishing time delay, i.e., $\phi = 0$.

In Fig. 6, we depict the spectra obtained for a diatomic molecule subjected to such a field, assuming either a two-center prefactor and the single-center saddle-point equation (35), or the modified saddle point equations (36)

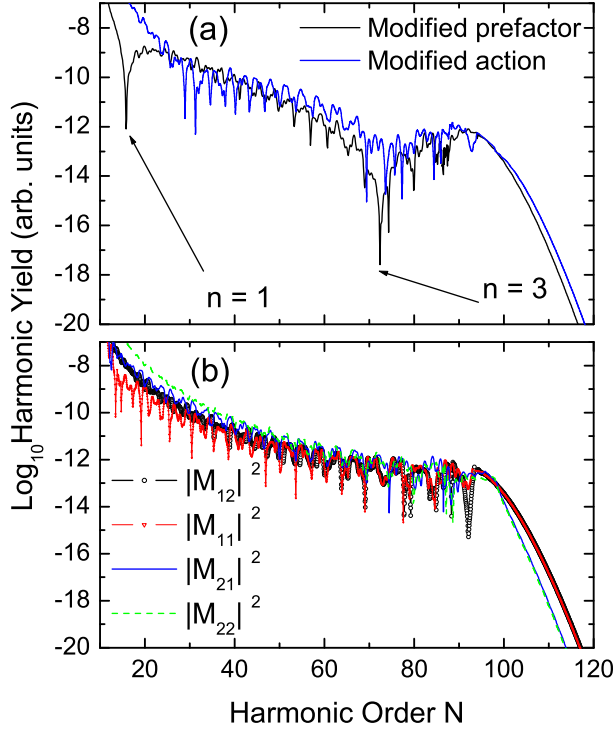


FIG. 6: (Color Online) High-harmonic spectra for a molecule aligned parallel to the laser-field polarization, and internuclear distance $R = 3.5$ a.u., for an attosecond pulse train superposed to a strong, near-infrared field, and exhibiting vanishing time-delay ($\phi = 0$) with respect to it. We consider a bonding combination of $1s$ atomic orbitals, and take the intensity of the attosecond-pulse train to be $I_h = I_l/10$. The remaining parameters are the same as in the previous figures. Panel (a): spectra computed employing the modified version of the two-center prefactors in the length form [Eq. (20)] and single-atom saddle-point equations, compared to that obtained using modified saddle-point equations. Panel (b): Contributions from individual scattering scenarios, i.e., from $|M_{j\nu}|^2$, with $j = 1, 2$ and $\nu = 1, 2$. The interference minima are indicated by arrows in the figure.

[Fig. 6.(a)]. Both computations exhibit a minimum near the harmonic frequency $\Omega = 71\omega$, in agreement with Eq. (17). If only the contributions $|M_{j\nu}|^2$ from the individual scattering scenarios are taken, such a minimum is absent [Fig. 6.(b)]. Therefore, it is due to interference effects between different sets of orbits. One should note that, in contrast to the purely monochromatic case, all contributions exhibit the same order of magnitude. This is due to the fact that, if the attosecond pulses are present, the electron is being ejected in the continuum with roughly the same probability, regardless of the center it left from.

The precise role of the various recombination scenarios is illustrated in Fig. 7. For clarity, we concentrate on the plateau region around the interference minimum. The main difference observed, with regard to the purely monochromatic case, is that the overall shape of the spectrum, and consequently its minimum, is due to the collec-

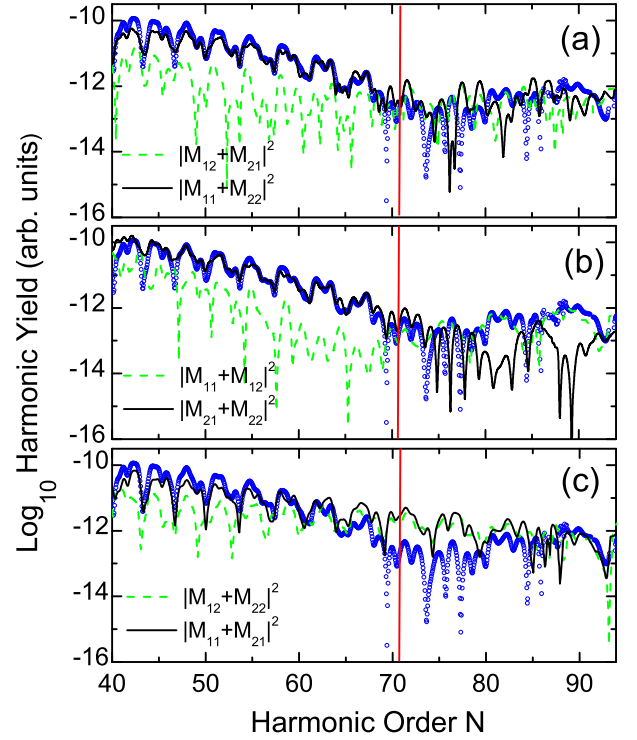


FIG. 7: (Color Online) Contributions to the high-harmonic yield from the quantum interference between different types of orbits, for the same field and molecular parameters as in Fig. 7. Panel (a): Contributions from topologically similar scattering scenarios, i. e., contributions from $|M_{11} + M_{22}|^2$ and $|M_{12} + M_{21}|^2$. Panel (b): Contributions from orbits starting at the same center. Panel (c): Contributions from orbits ending at the same center. For comparison, the overall spectra are displayed as the blue symbols in the figure. The interference minimum is indicated by the vertical lines near $\Omega = 71\omega$.

tive interference of several types of orbits. This is in contrast to the previous results, for which they were caused by the processes starting at a center C_j and ending at different centers, i.e., $|M_{j\nu} + M_{jj}|^2$, with $\nu \neq j$ and $\nu, j = (1, 2)$. Indeed, a modulation is even present for the probability $|M_{11} + M_{22}|^2$ involving only one-center scenarios. This is shown in Fig. 7.(a), and contradicts the previously made assumption that such features are due to the interference between topologically different sets of orbits. In fact, it seems that the absence of overall maxima and minima for the one-center contributions, in the purely monochromatic case [Fig. 3.(a)], is due to the different orders of magnitude for M_{11} and M_{22} [c.f. Fig. 4.(a)].

Furthermore, one needs several different processes in order to obtain the correct position of the minimum. For instance, in Fig. 7.(a), the overall spectrum closely follows $|M_{11} + M_{22}|^2$ in the low-energy region. In the vicinity of the minimum and for higher energies, however, it follows neither such contributions nor $|M_{12} + M_{21}|^2$, from two-center processes. In Fig. 7.(b), where we display the

contributions $|M_{jj} + M_{j\nu}|^2$, with $\nu \neq j$ and $\nu, j = (1, 2)$, from the orbits starting from the same center, the spectrum closely follows $|M_{21} + M_{22}|^2$ before the minimum, and $|M_{11} + M_{12}|^2$ after the minimum.

The remaining panel [Fig. 7.(c)] depicts the contributions from $|M_{\nu\nu} + M_{j\nu}|^2$, with $\nu \neq j$ and $\nu, j = (1, 2)$, which give the orbits *finishing* at the same center. In this case, the interference minimum is absent. This is a strong evidence that the relevant condition for the presence of such features is that the orbits taken into account end at different centers, instead of being topologically different (which is the case for both Fig. 7.(b) and Fig. 7.(c)). Therefore, these results agree with the double-slit picture, which has been put across in [18].

The additional attosecond pulses have the advantage of not introducing changes in the standard length-gauge SFA formulation. They modify, however, the physics of the problem, since they provide a different mechanism for the electron to reach the continuum. Clearly, there is also the possibility of eliminating the spurious potential energy shifts, by considering a different version of the SFA, such as the field-dressed length-gauge formulation proposed in [17], or the velocity-gauge formulation.

In Fig. 8, we display high-order harmonic spectra for the field-dressed SFA in the length gauge, and for the field-undressed SFA in the velocity gauge [panels (a) and (b), respectively]. For simplicity, we exhibit the results obtained with the modified prefactor (20), instead of a modified action. We also provide curves for which only the cosine term has been set to one, in order to facilitate the identification of interference effects. As an overall feature, we do not observe the interference patterns exhibited in the previous figures. Indeed, the curves with and without the cosine term are very similar. There is, however, a minimum near $\Omega = 115\omega$ for the former case.

For the dressed length-gauge SFA, the above-stated features can be attributed to the fact that the condition for maxima and minima is now given by (17), with \mathbf{p} instead of $\tilde{\mathbf{p}} = \mathbf{p} + \mathbf{A}(t)$. The harmonic frequencies for which they occur can be easily obtained from condition (6), and are given by

$$\Omega = I_p + [n^2\pi^2/R_x^2 + 2n\pi A(t)/R_x + A^2(t)]/2. \quad (38)$$

An upper bound for Ω can be estimated as follows. At the electron return times, the vector potential is roughly $A(t) \lesssim 2\sqrt{U_p}$. This yields, for the parameters in Fig. 8, $\Omega \sim 121\omega$, which is slightly larger than the minimum encountered.

A breakdown of the interference patterns also occurs in the velocity gauge, for the very same reasons. Indeed, the interference condition for the SFA in the velocity gauge and for the field-dressed SFA in the length gauge are identical. This is a direct consequence of the fact that field-free initial and final electron states in the velocity gauge are gauge-equivalent to the field-dressed states considered in this paper. This gauge equivalence will lead to identical recombination form factors $d_{\text{rec}}(\mathbf{p}) = \langle \mathbf{p} | \mathcal{O}_{\text{dip}} \cdot \mathbf{e}_x | \psi_0 \rangle$. Since the interference condi-

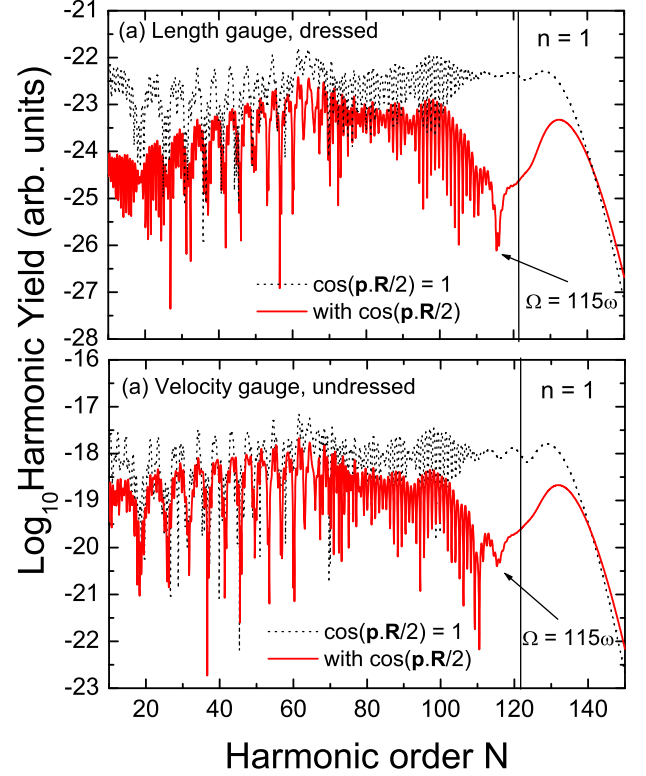


FIG. 8: (Color Online) High-order harmonic spectra for the same field and molecular parameters as in Fig. 2, but computed with the field-dressed modified length-gauge formulation of the strong-field approximation [Panel (a)], compared to its field-undressed velocity-gauge counterpart [Panel (b)]. The arrows in the figure indicate the harmonic order for which a minimum is observed, and the vertical line marks the rough estimate for such a minimum. The solid and dotted lines correspond to the prefactor (19) and to the situation for which $\cos \mathbf{p} \cdot \mathbf{R}/2$ has been set to one, respectively.

tions (17) are mainly determined by $d_{\text{rec}}(\mathbf{p})$, they will be the same. Hence, the harmonic orders for which the maxima and minima occur are given by Eq. (38), and therefore are unrealistically high. The discrepancies between both yields stem from the form factors $d_{\text{ion}}(\mathbf{p}) = \langle \mathbf{p} | H_{\text{int}}(t') | \psi_0 \rangle$, which are gauge-dependent.

One may, however, consider field-dressed states in the velocity gauge, which are gauge-equivalent to field-free states in the length gauge. This is achieved by applying the transformation $\chi_{v \leftarrow l} = \exp[i\mathbf{A}(t) \cdot \mathbf{r}]$ in the initial and final length-gauge electronic bound states. This leads to a shift $\mathbf{p} \rightarrow \mathbf{p} + \mathbf{A}(t)$ on a momentum eigenstate $|\mathbf{p}\rangle$, which is exactly the opposite shift induced in the field-dressed length-gauge SFA. This shift has the main consequence that the interference condition (17) now holds for $\tilde{\mathbf{p}} = \mathbf{p} + \mathbf{A}(t)$, even in the velocity gauge. The results

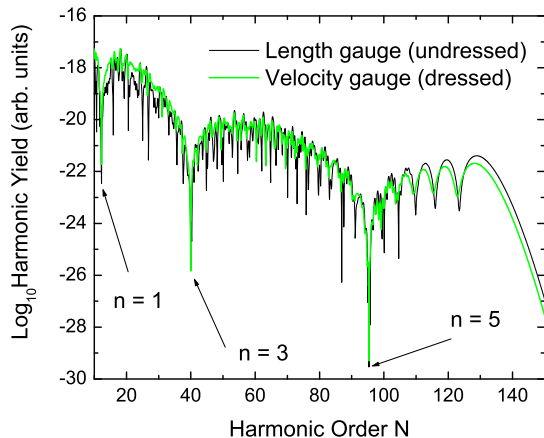


FIG. 9: (Color Online) High-order harmonic spectra for the same field and molecular parameters as in Fig. 2, but computed with the field-dressed modified velocity-gauge formulation of the strong-field approximation. In order to facilitate the comparison, the undressed length-gauge version of the SFA is provided, and the velocity-gauge yield has been normalized in approximately 2 orders of magnitude, to match the length-gauge results. In both cases, for simplicity, the modified prefactor (18) has been employed, instead of modified saddle-point equations.

obtained employing such dressed states in the velocity-gauge SFA, depicted in Fig. 9, are indeed very similar to those obtained using its field undressed, length gauge formulation. In fact, we have observed mainly quantitative differences, due to different prefactors $d_{\text{ion}}(\mathbf{p})$ [37].

One should note, however, that the transformation $\chi_{v \leftarrow l}$ introduces the same additional potential energy shifts in the modified action as in the undressed length-gauge case. Thus, the price one pays for recovering the correct interference conditions is the loss of a direct connection to simple classical models.

IV. CONCLUSIONS

The present results support the viewpoint that the maxima and minima in the high-order harmonic spectra of diatomic molecules are due to the interference of electron orbits finishing at different centers in the molecule. This seems to hold regardless of whether the electron has been released in one center at the molecule and recombines with a different center, or whether it is ejected and returns to the same center. Such conclusions have been reached by employing modified saddle-point equations, within the strong-field approximation. These modifications lead to orbits involving different centers, and are a slightly more refined approach than the standard procedure of considering single-center saddle-point equations

and modified prefactors.

In this framework, we considered that the electron has been ejected by tunneling ionization and by an additional attosecond-pulse train, and compared the similarities and differences from both physical situations. In the former case, depending from which center the electron is leaving, it must overcome unequal potential barriers to reach the continuum, whereas in the latter case it is ejected with roughly equal probability. Especially in the purely monochromatic case, we observed that the contributions from orbits starting at one of the centers, namely C_2 , were much larger than those from C_1 , due to a narrower potential barrier. In particular, there exist potential-energy shifts which are proportional to the electric field at the ionization time and the internuclear distance, which cause such differences. It is however noteworthy that the electron excursion times have been confined to the first half-cycle of the laser field. If the other half-cycle had been taken, the potential barrier would reverse and the contributions starting from C_1 would be more prominent.

The above-mentioned potential-energy shifts, however, do not possess a clear-cut physical interpretation. In fact, they are only present in the standard length-gauge formulation of the strong-field approximation, i.e., if field-free bound states are taken when the electron is ejected and recombines, and are the source of several problems. For instance, they reflect the fact that the SFA is translation-dependent. Moreover, due to their existence, it is difficult to establish an immediate connection between this approach and the classical equations of motion of an electron in the laser field.

On the other hand, it seems that such shifts are necessary in order to obtain the correct energy position of the maxima and minima in the HHG spectra. In fact, an improved formulation of the SFA, in which the influence of the laser field is included in the electron bound states, restores its translation invariance, provides an unproblematic classical limit [17], but yields incorrect energy positions for the interference patterns. This discrepancy is related to the fact that the field dressing alters the double-slit interference conditions (17). A similar absence of interference features has been reported very recently in Ref. [38], for HHG computations using a field-dressed version of the SFA in the length gauge.

Finally, when employing different gauges, from our results it is clear that the dressing of the initial and the final states plays a far more important role than the different interaction Hamiltonians $H_{\text{int}}(t')$. If the dressing is applied consistently so that the electronic bound states are gauge-equivalent, the interference patterns will remain the same. This is due to the fact that the interference condition (17) will then remain invariant. For instance, the spectra obtained in the velocity-gauge SFA with undressed states are very similar to those computed in the length gauge with field dressed states. The same holds for the undressed length-gauge, and the dressed velocity-gauge SFA spectra. In the two former cases, there is a breakdown of the interference patterns, as com-

pared to the field-undressed length gauge SFA. However, such patterns can be restored in the velocity gauge, by dressing the electronic bound states appropriately.

Acknowledgments

We would like to thank L. E. Chipperfield, R. Torres, J. P. Marangos, and H. Schomerus for useful discussions,

and W. Becker for calling Ref. [17] to our attention. We are also grateful to the Imperial College and to the University of Stellenbosch for their kind hospitality. This work has been financed by the UK EPSRC (Advanced Fellowship, Grant no. EP/D07309X/1).

-
- [1] J. Itatani, J. Levesque, D. Zeidler, H. Niikura, H. Pépin, J. C. Kieffer, P. B. Corkum and D. M. Villeneuve, *Nature* **432**, 867 (2004).
 - [2] H. Niikura, F. Légaré, R. Hasbani, A. D. Bandrauk, M. Yu. Ivanov, D. M. Villeneuve and P. B. Corkum, *Nature* **417**, 917 (2002); H. Niikura, F. Légaré, R. Hasbani, M. Yu. Ivanov, D. M. Villeneuve and P. B. Corkum, *Nature* **421**, 826 (2003); S. Baker, J. S. Robinson, C. A. Haworth, H. Teng, R. A. Smith, C. C. Chirilă, M. Lein, J. W. G. Tisch, J. P. Marangos, *Science* **312**, 424 (2006).
 - [3] A. Scrinzi, M. Y. Ivanov, R. Kienberger, and D. M. Villeneuve, *J. Phys. B* **39**, R1 (2006).
 - [4] P. B. Corkum, *Phys. Rev. Lett.* **71**, 1994 (1993); K. C. Kulander, K. J. Schafer, and J. L. Krause in: B. Piraux et al. eds., *Proceedings of the SILAP conference*, (Plenum, New York, 1993).
 - [5] R. Kopold, W. Becker and M. Kleber, *Phys. Rev. A* **58**, 4022 (1998).
 - [6] J. Muth-Böhm, A. Becker, and F. H. M. Faisal, *Phys. Rev. Lett.* **85**, 2280 (2000); A. Jarón-Becker, A. Becker, and F. H. M. Faisal, *Phys. Rev. A* **69**, 023410 (2004); A. Requate, A. Becker and F. H. M. Faisal, *Phys. Rev. A* **73**, 033406 (2006).
 - [7] T. K. Kjeldsen and L. B. Madsen, *J. Phys. B* **37**, 2033 (2004); *Phys. Rev. A* **71**, 023411 (2005); *Phys. Rev. Lett.* **95**, 073004 (2005); T. K. Kjeldsen, C. Z. Bisgaard, L. B. Madsen, H. Stapelfeld, *Phys. Rev. A* **71**, 013418 (2005); C. B. Madsen and L. B. Madsen, *Phys. Rev. A* **74**, 023403 (2006).
 - [8] V. I. Usachenko, and S. I. Chu, *Phys. Rev. A* **71**, 063410 (2005).
 - [9] H. Hetzheim, M. Sc. thesis (Humboldt University Berlin, 2005).
 - [10] V. I. Usachenko, P. E. Pyak, and Shih-I Chu, *Laser Phys.* **16**, 1326 (2006).
 - [11] C. C. Chirilă and M. Lein, *Phys. Rev. A* **73**, 023410 (2006).
 - [12] M. Lein, *Phys. Rev. Lett.* **94**, 053004 (2005); C. C. Chirilă and M. Lein, *J. Phys. B* **39**, S437 (2006).
 - [13] H. Hetzheim, C. Figueira de Morisson Faria, and W. Becker *Phys. Rev. A*, in press (arXiv:0704.0712).
 - [14] S. X. Hu and L. A. Collins, *Phys. Rev. Lett.* **94**, 073004 (2005); D. A. Telnov and Shih-I Chu, *Phys. Rev. A* **71**, 013408 (2005).
 - [15] G. Lagmago Kamta and A. D. Bandrauk, *Phys. Rev. A* **70**, 011404 (2004); *ibid.* **71**, 053407 (2005).
 - [16] X. Zhou, X. M. Tong, Z. X. Zhao and C. D. Lin, *Phys. Rev. A* **71**, 061801(R) (2005); *ibid.* **72**, 033412 (2005).
 - [17] D. B. Milošević, *Phys. Rev. A* **74**, 063404 (2006).
 - [18] M. Lein, N. Hay, R. Velotta, J. P. Marangos, and P. L. Knight, *Phys. Rev. Lett.* **88**, 183903 (2002); *Phys. Rev. A* **66**, 023805 (2002); M. Spanner, O. Smirnova, P. B. Corkum and M. Y. Ivanov, *J. Phys. B* **37**, L243 (2004).
 - [19] B. Shan, X. M. Tong, Z. Zhao, Z. Chang, and C. D. Lin, *Phys. Rev. A* **66**, 061401(R) (2002); F. Grasbon, G. G. Paulus, S. L. Chin, H. Walther, J. Muth-Böhm, A. Becker and F. H. M. Faisal, *Phys. Rev. A* **63**, 041402(R) (2001); C. Altucci, R. Velotta, J. P. Marangos, E. Heesel, E. Springate, M. Pascolini, L. Poletto, P. Villoresi, C. Vozzi, G. Sansone, M. Anscombe, J. P. Caumes, S. Stagira, and M. Nisoli, *Phys. Rev. A* **71**, 013409 (2005); T. Kanai, S. Minemoto and H. Sakai, *Nature* **435**, 470 (2005).
 - [20] C. C. Chirilă and M. Lein, *J. Mod. Opt.* **54**, 1039 (2007).
 - [21] K. J. Schafer, M. B. Gaarde, A. Heinrich, J. Biegert, and U. Keller, *Phys. Rev. Lett.* **92**, 023003 (2004); M. B. Gaarde, K. J. Schafer, A. Heinrich, J. Biegert, and U. Keller, *Phys. Rev. A* **72**, 013411 (2005); J. Biegert, A. Heinrich, C. P. Hauri, W. Kornelis, P. Schlup, M. P. Anscombe, M. B. Gaarde, K. J. Schafer and U. Keller, *J. Mod. Opt.* **53**, 87 (2006); J. Biegert, A. Heinrich, C. P. Hauri, W. Kornelis, P. Schlup, M. P. Anscombe, K. J. Schafer, M. B. Gaarde and U. Keller, *Laser Physics* **15**, 899 (2005).
 - [22] P. Johnsson, R. López-Martens, S. Kazamias, J. Mauritsson, C. Valentin, T. Remetter, K. Varjú, M. B. Gaarde, Y. Mairesse, H. Wabnitz, P. Salières, Ph. Balcou, K. J. Schafer, and A. L'Huillier, *Phys. Rev. Lett.* **95**, 013001 (2005); P. Johnsson, K. Varjú, T. Remetter, E. Gustafsson, J. Mauritsson, R. Lopez-Martens, S. Kazamias, C. Valentin, Ph. Balcou, M. B. Gaarde, K. J. Schafer, and A. L'Huillier, *J. Mod. Opt.* **53**, 233 (2006).
 - [23] C. Figueira de Morisson Faria, P. Salières, P. Villain and M. Lewenstein, *Phys. Rev. A* **74**, 053416 (2006).
 - [24] C. Figueira de Morisson Faria and P. Salières, *Laser Phys.* **17**, 390 (2007).
 - [25] W. Becker, S. Long, and J. K. McIver *Phys. Rev. A* **50**, 1540 (1994).
 - [26] M. Lewenstein, Ph. Balcou, M. Yu. Ivanov, A. L'Huillier and P. B. Corkum, *Phys. Rev. A* **49**, 2117 (1994).
 - [27] W. Becker, S. Long, and J. K. McIver, *Phys. Rev. A* **41**, 4112 (1990); *ibid.* **50**, 1540 (1994); M. Lewenstein, K. C. Kulander, K. J. Schafer and Ph. Bucksbaum, *Phys. Rev. A* **51**, 1495 (1995).
 - [28] W. Becker, A. Lohr, M. Kleber, and M. Lewenstein, *Phys. Rev. A* **56**, 645 (1997).
 - [29] P. Salières, B. Carré, L. LeDéroff, F. Grasbon, G. G. Paulus, H. Walther, R. Kopold, W. Becker, D. B. Milošević, A. Sanpera and M. Lewenstein, *Science* **292**, 902 (2001).
 - [30] A. Fring, V. Kostykin and R. Schrader, *J. Phys. B*, **29**,

- 5651 (1996); D. Bauer, D. B. Milošević and W. Becker, Phys. Rev. A **72**, 023415 (2005).
- [31] In the length or velocity gauge, this interaction is given by $H_I^L(t') = \mathbf{r} \cdot \mathbf{E}(t')$ or $H_I^V(t') = [\mathbf{p} + \mathbf{A}(t')]^2/2$, respectively.
- [32] O. Smirnova, M. Spanner and M. Ivanov, J. Phys. B **39**, S307 (2006).
- [33] C. Figueira de Morisson Faria, H. Schomerus and W. Becker, Phys. Rev. A **66**, 043413 (2002).
- [34] K. Burnett, V. C. Reed, J. Cooper and P. L. Knight, Phys. Rev. A **45**, 3347 (1992); J. L. Krause, K. Schafer and K. Kulander, Phys. Rev. A **45**, 3347 (1992).
- [35] Since the bound state with which the returning electron recombines is highly localized, a broader wave packet means a less pronounced overlap upon recombination and, consequently, weaker harmonics.
- [36] C. Figueira de Morisson Faria, X. Liu, A. Sanpera and M. Lewenstein, Phys. Rev. A **70**, 043406 (2004).
- [37] In these SFA formulations, for exponentially decaying states, $\phi(\tilde{\mathbf{p}})$ and $\partial_{p_x} \phi(\tilde{\mathbf{p}})$ exhibit a singularity, which can be eliminated by being incorporated in the action. This has not been included in our model, and may lead to further differences between both yields. We expect, however, these discrepancies to be minimal, as this additional term is slowly varying. For a discussion in the length-gauge context, c.f., C. Figueira de Morisson Faria and M. Lewenstein, J. Phys. B **38**, 3251 (2005).
- [38] O. Smirnova, M. Spanner and M. Ivanov, J. Mod. Opt. **54**, 1019 (2007).